Theory of excitonic confinement in semiconductor quantum wires

1999 J. Phys.: Condens. Matter 11 5969

(http://iopscience.iop.org/0953-8984/11/31/306)

J. Phys.: Condens. Matter **11** (1999) 5969–5988. Printed in the UK PII: S0953-8984(99)01597-0

Theory of excitonic confinement in semiconductor quantum wires

Fausto Rossi†‡§, Guido Goldoni†‡, Oskar Mauritz†‡ and Elisa Molinari†‡

† Istituto Nazionale per la Fisica della Materia (INFM), Italy
‡ Dipartimento di Fisica, Università di Modena e Reggio Emilia, Via Campi 213/A, I-41100 Modena, Italy
§ Dipartimento di Fisica, Politecnico di Torino, Corso Duca degli Abruzzi 24, I-10129 Torino, Italy

Received 4 February 1999

Abstract. We review our theoretical approach to the optical response of low-dimensional semiconductor structures. The method is based on the density-matrix formalism and can treat low-density (excitonic) and high-density (gain) regimes on the same footing while retaining the full complexity of realistic nanostructures. We discuss in particular its generalization for studying the combined effects of dielectric and quantum confinement, as well as novel developments aimed at the analysis of local absorption spectra.

We examine the main effects of electron–hole Coulomb correlation on the optical spectra of semiconductor quantum wires, where it determines the suppression of band-edge singularities and the peculiar scaling properties of excitonic binding and non-linearities. On the basis of our recent results on different types of nanostructure, we present a critical discussion of possible strategies for tailoring electron–hole Coulomb interaction, and predicting its influence on near-field spectra.

1. Introduction

During the last decade the optical properties of quasi-one-dimensional structures, the so-called quantum wires (QWRs), have become a topic of increasing interest. The initial motivation was related to the one-dimensional (1D) singularity in the single-particle density of states (DOS), that was expected to induce sharp peaks in the optical spectra, thereby leading to structures with improved optical efficiency as compared to their two-dimensional (2D) and three-dimensional (3D) counterparts [1].

Coulomb correlations strongly modify this simple picture. This was first pointed out by Ogawa and Takagahara [2], using an idealized 1D model. More recently, calculations have been performed [3] within a fully 3D approach based on the density-matrix formalism, which results in a set of generalized (multisubband) semiconductor Bloch equations (SBE) [4–6]. This method is able to treat both low-density (excitonic) and high-density (gain) regimes on the same footing, while retaining the full complexity of state-of-the-art samples. For example, it has been used to describe structures obtained by epitaxial growth on non-planar substrates (V-shaped wires) [1, 7–9] or by cleaved-edge quantum well overgrowth (T-shaped wires) [10–12], where the lateral extension of the ground single-particle states is still significant, the excited states gradually approach a 2D-like behaviour, and the subband separation is relatively small, so the coupling between different subbands may be important.

0953-8984/99/315969+20$30.00

Our calculations [3] have shown that

(a) The correlated absorption spectra of realistic wires do show a strong quenching of the 1D single-particle singularity, in agreement with reference [2]; this effect does not depend on details of the wire cross-section. The Sommerfeld factor, which is greater than unity for the bulk and in quantum wells (the so-called Coulomb enhancement), is instead smaller than unity for QWRs (Coulomb suppression), thus reducing the influence of dimensionality on the optical spectra.
(b) The Coulomb-induced suppression of the 1D singularity is found to hold not only in the linear regime but also at higher carrier densities, and to persist in the gain regime.

The above results have had implications for prospective devices, since the initial motivations—based on single-particle models—are now recognized as being far too simplified. Given the Coulomb-induced suppression of the band-edge singularity, the most relevant features arising from electron–hole correlation are bound- (below-band-gap) excitonic states, which, for relatively low carrier densities, are found to dominate the optical response of the system. Therefore one of the most important goals is now the achievement of a large exciton binding energy E_b, as compared to the thermal energy kT_{room}: this is indeed a prerequisite for exploiting excitonic non-linearities in optical devices that can operate efficiently at room temperature.

In principle, enhancing E_b in QWRs is an easy task: in quasi-1D (q1D) structures, in fact, E_b can be made arbitrarily large [13] provided that one is able to squeeze the electron and hole wavefunctions to a sufficient extent, thereby increasing the Coulomb energy. Note that this contrasts with the case for 2D systems, for which, even in the ideal case of perfect 2D confinement, the binding energy of the ground-state exciton is limited to four times the 3D effective rydberg. In practice, for the materials of choice for technological application—GaAs/AlAs—this strategy is difficult to implement. While for quantum wells (QWs) E_b has indeed been observed to approach the theoretical limit when the well thickness is progressively reduced [14], for QWRs the reported values of E_b are only slightly larger than for QWs, and still well below kT_{room}. In fact, the strong confinement regime which is necessary to enhance the relatively low value of E_b for bulk GaAs ($\sim$4 meV) is still hard to obtain with the relatively shallow confinements permitted by present GaAs/AlAs-based structures. Despite the substantial recent experimental effort, this limitation makes order-kT_{room} exciton binding energy a difficult goal.

A discussion of the intrinsic limitations of E_b for realistic QWRs is therefore important. It should be noted that for a given confinement length (i.e., electron–hole Coulomb interaction energy), E_b is determined by the Coulomb-to-kinetic-energy ratio, whose value is fixed to -2 for purely 2D and 3D Coulombic systems; since this ratio is ill-defined for purely 1D Coulombic systems (both kinetic and Coulomb energies diverge) and, moreover, the virial theorem does not hold in the presence of a confining potential, it might be hoped that a more convenient (i.e., smaller) ratio could be obtained for properly designed structures. In this spirit, we have recently performed [15] a detailed investigation of excitonic confinement for a wide class of state-of-the-art GaAs/AlGaAs QWRs, with the aim of investigating whether, in addition to the squeezing of the wavefunction (which, as we have discussed, is somewhat limited by the choice of the materials), geometrical tailoring of the structure could be used to enhance the binding energy. Our results show that, in general, q1D systems are indeed advantageous with respect to 2D ones, since smaller Coulomb-to-kinetic-energy ratios are possible in the former system in the strong-confinement limit. However, such deviations scale in a universal manner with respect to the wire cross-section. Consistently, for all GaAs-based QWRs structures considered, E_b is found to be very similar and always smaller than kT_{room}.

Motivated by these results, we have recently proposed an alternative approach to enhance E_b [16], which combines the effects of *quantum confinement* discussed so far, with those of *dielectric confinement*, i.e., confinement effects induced by dielectric mismatch. As first pointed out by Keldysh [17], the electron–hole Coulomb attraction can be greatly enhanced in layered structures with strong dielectric mismatch, due to the polarization charge induced at the interfaces. For conventional semiconductor nanostructures such as GaAs/AlGaAs- or GaAs/InGaAs-based samples, this is a minor effect due to the small dielectric mismatch between the constituents [18]. On the other hand, interfaces between III–V semiconductors and materials with very different dielectric constants, such as oxides, are usually very far from the excellent optical quality of the conventional ones. The proposed approach is based on the idea that *quantum and dielectric confinement can be spatially separated*, since they are effective over different length scales. This may be achieved by adding to a conventional semiconductor QWR remote insulating layers which may induce strong dielectric confinement without degrading the good optical properties ensuing from quantum confinement, hence the term *remote dielectric confinement* (RDC).

When dielectrically modulated structures are investigated, the electron–hole interaction is no longer the bare Coulomb interaction; instead, it must be explicitly calculated, for a given structure, as the Green's function of the Laplace operator with a spatially dependent dielectric constant. Accordingly, we have generalized our multisubband SBE approach described in [3] in order to include such renormalized electron–hole interaction as well as self-energy effects. In reference [15] we have shown that RDC applied to state-of-the-art GaAs/AlAs-based QWRs may allow room-temperature exciton binding.

On very general grounds, RDC can be seen as a practical method for enhancing the electron–electron and electron–hole interaction within the wire, without disturbing the quantum-confined single-particle states (apart from the small self-energy effects, to be discussed in detail later). One is therefore tailoring the Coulomb interaction, similarly to what is done—although in the opposite direction—by use of screening from free carriers. In this respect, we expect that RDC might find other fields of application in the transport and many-body properties in q1D systems.

The aim of this paper is to provide a critical review of the properties of excitonic confinement in realistic semiconductor QWRs. After a comprehensive description of the theoretical approach adopted in references [3, 15, 16, 19], we discuss the resulting physical picture paying particular attention to the interplay between quantum and dielectric confinement, as a potential strategy for achieving exciton binding at room temperature, and to local excitation optical spectra of coupled QWR structures.

2. Theory of linear and non-linear optical response in quantum wires

In this section we review and discuss our theoretical approach to the study of the linear and non-linear optical response of low-dimensional semiconductor structures. The proposed density-matrix formulation allows us to study both *global* and *local* optical excitations and can be generalized to include effects due to *remote dielectric confinement*.

In order to investigate the optical response of a semiconductor structure, the key quantity to be evaluated is the optical polarization field, i.e., the degree of polarization induced in the carrier system by the optical excitation. From a microscopic point of view, the local (i.e., space-dependent) polarization can be written as

$$\boldsymbol{P}(\boldsymbol{r},t) = e\left\langle \hat{\boldsymbol{\Psi}}^{\dagger}(\boldsymbol{r},t)\boldsymbol{r}\hat{\boldsymbol{\Psi}}(\boldsymbol{r},t)\right\rangle \tag{1}$$

where e is the electronic charge, $\langle\cdots\rangle$ denotes a proper ensemble average, and the field operator

$\hat{\boldsymbol{\Psi}}(\boldsymbol{r}, t)$ in the Heisenberg picture describes the microscopic time evolution of the carrier system.

Since in this paper we focus on optical excitations, it is convenient to work within the so-called electron–hole picture. This corresponds to writing the field operator $\hat{\boldsymbol{\Psi}}(\boldsymbol{r}, t)$ as a linear combination of single-particle electron and hole states (Ψ_i and Ψ_j):

$$\hat{\boldsymbol{\Psi}}(\boldsymbol{r}) = \sum_i \hat{c}_i \Psi_i(\boldsymbol{r}) + \sum_j \hat{d}_j^\dagger \Psi_j^*(\boldsymbol{r}) \tag{2}$$

where $\hat{c}_i$ and $\hat{d}_j$ denote destruction operators for an electron in state i and a hole in state j. Here, i and j are appropriate sets of quantum numbers which label the single-particle wavefunctions $\Psi_{i/j}$ and energy levels $\epsilon_{i/j}$ involved in the optical transition.

By inserting the above electron–hole expansion into equation (1), and neglecting intraband contributions (absent for the case of optical excitations), the local polarization can be rewritten as

$$\boldsymbol{P}(\boldsymbol{r}, t) = \sum_{ij} \left[\boldsymbol{M}_{ij}^*(\boldsymbol{r}) p_{ij}(t) + \text{c.c.} \right] \tag{3}$$

where

$$\boldsymbol{M}_{ij}(\boldsymbol{r}) = e \Psi_i^*(\boldsymbol{r}) \boldsymbol{r} \Psi_j^*(\boldsymbol{r}) \tag{4}$$

is the local (i.e. space-dependent) dipole matrix element, and

$$p_{ji} = \langle \hat{d}_j \hat{c}_i \rangle \tag{5}$$

are non-diagonal (i.e. interband) elements of the single-particle density matrix, also referred to as interband polarizations.

The time evolution of the above interband polarizations p_{ji} is governed by the so-called semiconductor Bloch equations (SBE) [4, 20, 21]:

$$\begin{aligned}
\frac{\partial}{\partial t} f_i &= \frac{1}{\mathrm{i}\hbar} \sum_{j'} (\mathcal{U}_{ij'} p_{j'i}^* - \mathcal{U}_{ij'}^* p_{j'i}) + \left. \frac{\partial f_i}{\partial t} \right|_{inco} \\
\frac{\partial}{\partial t} f_j &= \frac{1}{\mathrm{i}\hbar} \sum_{i'} (\mathcal{U}_{i'j} p_{ji'}^* - \mathcal{U}_{i'j}^* p_{ji'}) + \left. \frac{\partial f_j}{\partial t} \right|_{inco} \\
\frac{\partial}{\partial t} p_{ji} &= \frac{1}{\mathrm{i}\hbar} \sum_{i'j'} (\mathcal{E}_{ii'} \delta_{jj'} + \mathcal{E}_{jj'} \delta_{ii'}) p_{j'i'} + \frac{1}{\mathrm{i}\hbar} \mathcal{U}_{ij} (1 - f_i - f_j) + \left. \frac{\partial p_{ji}}{\partial t} \right|_{inco}
\end{aligned} \tag{6}$$

where $f_i = \langle \hat{c}_i^\dagger \hat{c}_i \rangle$ and $f_j = \langle \hat{d}_j^\dagger \hat{d}_j \rangle$ denote electron and hole distribution functions, i.e., diagonal density-matrix elements. Here,

$$\mathcal{U}_{ij} = U_{ij} - \sum_{i'j'} V_{ij'ji'} p_{j'i'} \tag{7}$$

and

$$\begin{aligned}
\mathcal{E}_{ii'} &= \epsilon_i \delta_{ii'} - \sum_{i''} V_{ii''i'i''} f_{i''} \\
\mathcal{E}_{jj'} &= \epsilon_j \delta_{jj'} - \sum_{j''} V_{jj''j'j''} f_{j''}
\end{aligned} \tag{8}$$

are, respectively, the Rabi and electron/hole energies renormalized by the Coulomb interaction [4, 20, 21]. The general form of the 'undressed' Rabi frequency U in (7) induced by a space- and time-dependent light field $\boldsymbol{E}(\boldsymbol{r}, t)$ is

$$U_{ij}(t) = -\int \boldsymbol{M}_{ij}(\boldsymbol{r}) \cdot \boldsymbol{E}(\boldsymbol{r}, t) \, \mathrm{d}\boldsymbol{r}. \tag{9}$$

Here, the V are full three-dimensional Coulomb matrix elements within the electron–hole (ij) single-particle representation. The last term in equation (6) accounts for incoherent (i.e., scattering and diffusion) processes. They do not play a central role for the physical phenomena discussed in the present paper; therefore, they will be simply treated within the usual relaxation-time approximation.

In order to study both global and local optical spectra, as a first step one needs to evaluate the stationary solutions of the SBE (6). They can easily be found in the so-called quasi-equilibrium regime, i.e. by assuming equilibrium distribution functions f_i, f_j; as described in [3], the equation of motion for the interband polarization p_{ij} can be transformed into an eigenvalue problem (within the single-particle basis ij), whose λth solution, describing excitonic states, provides the complex energy eigenvalue $\Sigma^\lambda = \hbar\omega^\lambda - \mathrm{i}\Gamma^\lambda$ and the corresponding eigenvector $\boldsymbol{c}^\lambda$. The eigenvector components c_{ij}^λ can be regarded as matrix elements of the unitary transformation S connecting our original single-particle basis ij with the excitonic basis λ:

$$c_{ij}^\lambda = S_{ij,\lambda} = \langle ij|\lambda\rangle. \tag{10}$$

The desired stationary solutions within this new excitonic picture λ are given by

$$p(t) = p^\lambda \mathrm{e}^{\Sigma^\lambda t/\mathrm{i}\hbar} \tag{11}$$

with

$$p^\lambda = \frac{1}{\mathrm{i}\hbar}\sum_{ij} c_{ij}^{\lambda *} U_{ij}(\omega^\lambda)(1 - f_i - f_j) \tag{12}$$

where $U_{ij}(\omega)$ is the Fourier transform of the Rabi energy in (13).

2.1. Global response analysis

For the case of a homogeneous (i.e. space-independent) optical excitation $\boldsymbol{E}^o$ the Rabi energy U_{ij} in equation (9) (within the dipole approximation) is given by

$$U_{ij}(t) = -\bar{\boldsymbol{M}}_{ij} \cdot \boldsymbol{E}(t) \tag{13}$$

where

$$\bar{\boldsymbol{M}}_{ij} = \int \boldsymbol{M}_{ij}(\boldsymbol{r})\,\mathrm{d}\boldsymbol{r} \tag{14}$$

is the total dipole matrix element. Moreover, for the case of a homogeneous excitation the key quantity—the one measured experimentally—is the total polarization of the system, given by the space integral of the local polarization field in (3):

$$\bar{\boldsymbol{P}}(t) = \int \boldsymbol{P}(\boldsymbol{r}, t)\,\mathrm{d}\boldsymbol{r} = \sum_{ij}\left[\bar{\boldsymbol{M}}_{ij}^* p_{ij}(t) + \text{c.c.}\right]. \tag{15}$$

The global (linear as well as non-linear) absorption spectrum is obtained as the imaginary part of the optical susceptibility. This, in turn, is related to the Fourier transform of the above total polarization, which in the excitonic picture λ can be rewritten as

$$\bar{\boldsymbol{P}}(t) = \sum_\lambda \left[\bar{\boldsymbol{M}}^{\lambda *} p^\lambda(t) + \text{c.c.}\right] \tag{16}$$

with

$$\bar{\boldsymbol{M}}^\lambda = \sum_{ij} c_{ij}^{\lambda *} \bar{\boldsymbol{M}}_{ij}. \tag{17}$$

By inserting the stationary solution (11) as well as the dipole matrix element (17) into equation (15) and then taking its Fourier transform, we get

$$\bar{\boldsymbol{P}}(\omega) = -\mathrm{i}\bar{h}\sum_{\lambda}\frac{\bar{\boldsymbol{M}}^{\lambda *}p^{\lambda}}{\Sigma^{\lambda}-\bar{h}\omega} = -\sum_{\lambda,ij,i'j'}\frac{c_{ij}^{\lambda}\bar{\boldsymbol{M}}_{ij}^{*}c_{i'j'}^{\lambda *}U_{i'j'}(1-f_i-f_j)}{\Sigma^{\lambda}-\bar{h}\omega}. \tag{18}$$

Substituting the explicit form of the Rabi energy U we finally get

$$\bar{\boldsymbol{P}}(\omega) = \bar{\chi}(\omega)\cdot\boldsymbol{E}(\omega) \tag{19}$$

with

$$\bar{\chi}(\omega) = \sum_{\lambda,ij,i'j'}\frac{c_{ij}^{\lambda}\bar{\boldsymbol{M}}_{ij}^{*}\times c_{i'j'}^{\lambda *}\bar{\boldsymbol{M}}_{i'j'}(1-f_i-f_j)}{\Sigma^{\lambda}-\bar{h}\omega}. \tag{20}$$

This is the desired microscopic expression for the susceptibility tensor $\bar{\chi}$, whose imaginary part is proportional to the global absorption spectrum:

$$\bar{\boldsymbol{\alpha}}(\omega) \propto \Im\left[\bar{\chi}(\omega)\right]. \tag{21}$$

2.2. Local response analysis

Let us now consider the case of a local (i.e. space-dependent) optical excitation $\boldsymbol{E}(\boldsymbol{r})$. Contrary to the homogeneous excitation case, the electromagnetic field cannot be factorized as in equation (13), and the Rabi energy U should be evaluated according to the general expression (9). Similarly, in order to investigate the space-dependent response of the system through a local optical excitation, we need to evaluate the local (rather than the total) polarization field given by (3), which can be written again in our λ-representation as

$$\boldsymbol{P}(\boldsymbol{r},t) = \sum_{\lambda}\left[\boldsymbol{M}^{\lambda *}(\boldsymbol{r})p^{\lambda}(t) + \text{c.c.}\right] \tag{22}$$

with

$$\boldsymbol{M}^{\lambda}(\boldsymbol{r}) = \sum_{ij}c_{ij}^{\lambda *}\boldsymbol{M}_{ij}(\boldsymbol{r}). \tag{23}$$

By inserting the stationary solution (11) as well as the dipole matrix element (23) into equation (22) and then taking its Fourier transform, we get

$$\boldsymbol{P}(\boldsymbol{r},\omega) = -\mathrm{i}\bar{h}\sum_{\lambda}\frac{\boldsymbol{M}^{\lambda *}(\boldsymbol{r})p^{\lambda}}{\Sigma^{\lambda}-\bar{h}\omega} = -\sum_{\lambda,ij,i'j'}\frac{c_{ij}^{\lambda}\boldsymbol{M}_{ij}^{*}(\boldsymbol{r})c_{i'j'}^{\lambda *}U_{i'j'}(1-f_i-f_j)}{\Sigma^{\lambda}-\bar{h}\omega}. \tag{24}$$

Using the explicit form of the Rabi energy in (9), we finally get

$$\boldsymbol{P}(\boldsymbol{r},\omega) = \int \mathrm{d}\boldsymbol{r}'\,\boldsymbol{\chi}(\boldsymbol{r},\boldsymbol{r}',\omega)\cdot\boldsymbol{E}(\boldsymbol{r},\omega) \tag{25}$$

where

$$\boldsymbol{\chi}(\boldsymbol{r},\boldsymbol{r}',\omega) = \sum_{\lambda,ij,i'j'}\frac{c_{ij}^{\lambda}\boldsymbol{M}_{ij}^{*}(\boldsymbol{r})\times c_{i'j'}^{\lambda *}\boldsymbol{M}_{i'j'}(\boldsymbol{r}')(1-f_i-f_j)}{\Sigma^{\lambda}-\bar{h}\omega} \tag{26}$$

is the desired microscopic expression for our space-dependent susceptibility tensor.

For semiconductor structures described within the usual envelope-function formalism with isotropic electron and hole bulk dispersions, the local dipole matrix element $\boldsymbol{M}_{ij}(\boldsymbol{r})$ given by (4) is simply given by

$$\boldsymbol{M}_{ij}(\boldsymbol{r}) = \boldsymbol{M}_b\psi_i^{*}(\boldsymbol{r})\psi_j^{*}(\boldsymbol{r}) \tag{27}$$

where $\psi_{i/j}(\boldsymbol{r})$ are single-particle electron/hole envelope functions and M_b is the bulk dipole matrix element. Within such an approximation scheme, the susceptibility tensor $\boldsymbol{\chi}$ in (26) becomes diagonal, with identical elements given by

$$\chi(\boldsymbol{r},\boldsymbol{r}',\omega) = |M_b|^2 \sum_{\lambda,ij,i'j'} c_{ij}^{\lambda} c_{i'j'}^{\lambda *}(1-f_{i'}-f_{j'}) \frac{\psi_i(\boldsymbol{r})\psi_j(\boldsymbol{r})\psi_{i'}^*(\boldsymbol{r}')\psi_{j'}^*(\boldsymbol{r}')}{\Sigma^{\lambda}-\overline{h}\omega}. \tag{28}$$

Given the susceptibility function in (28), the total absorption power in a generic semiconductor structure can be evaluated according to

$$\alpha(\omega) \propto \int \mathrm{d}\boldsymbol{r} \int \mathrm{d}\boldsymbol{r}' \, \Im\left[E(\boldsymbol{r},\omega)\chi(\boldsymbol{r},\boldsymbol{r}',\omega)E(\boldsymbol{r}',\omega)\right]. \tag{29}$$

In the usual definition of the absorption coefficient within the dipole approximation given in equation (21) the non-locality of χ is neglected: $\chi(\boldsymbol{r},\boldsymbol{r}') \propto \delta(\boldsymbol{r}-\boldsymbol{r}')$. When non-locality is taken into account, it is no longer possible to define an absorption coefficient that locally relates the absorbed power density to the light intensity.

However, considering a light field with a given profile ξ centred around the beam position $\boldsymbol{R}$, $E(\boldsymbol{r},\omega) = E(\omega)\xi(\boldsymbol{r}-\boldsymbol{R})$, we may define a local absorption that is a function of the beam position, and relates the *total* absorbed power to the power of a *local* excitation (illumination mode):

$$\alpha_{\xi}(\boldsymbol{R},\omega) \propto \int \Im\left[\chi(\boldsymbol{r},\boldsymbol{r}',\omega)\right]\xi(\boldsymbol{r}-\boldsymbol{R})\xi(\boldsymbol{r}'-\boldsymbol{R})\,\mathrm{d}\boldsymbol{r}\,\mathrm{d}\boldsymbol{r}'. \tag{30}$$

This expression is in principle not limited to low photoexcitation intensities; together with equation (28) it provides a general description of linear as well as non-linear local response, i.e., from excitonic absorption to the gain regime.

In the linear response regime, $1-f_i-f_j \simeq 1$, and the quantity

$$\Psi^{\lambda}(\boldsymbol{r}_e,\boldsymbol{r}_h) = \sum_{ij} c_{ij}^{\lambda}\psi_i(\boldsymbol{r}_e)\psi_j(\boldsymbol{r}_h) \tag{31}$$

can be identified with the exciton wavefunction; in this case the explicit form of the local absorption coefficient (30) is given by

$$\alpha_{\xi}(\boldsymbol{R},\omega) = \sum_{\lambda} \alpha_{\xi}^{\lambda}(\boldsymbol{R},\omega) \tag{32}$$

where

$$\alpha_{\xi}^{\lambda}(\boldsymbol{R},\omega) \propto \left| \int \Psi^{\lambda}(\boldsymbol{r},\boldsymbol{r})\xi(\boldsymbol{r}-\boldsymbol{R})\,\mathrm{d}\boldsymbol{r} \right|^2. \tag{33}$$

The effects of spatial coherence of quantum states are easily understood in the linear regime on the basis of equation (33). For a spatially homogeneous electromagnetic (EM) field, the absorption spectrum probes the average of Ψ^{λ} over the whole space (global spectrum). In the opposite limit of an infinitely narrow probe beam, α maps $|\Psi^{\lambda}|^2$; the local absorption is non-zero at any point where the exciton wavefunction gives a finite contribution. It is therefore clear that 'forbidden' excitonic transitions, not present in the global spectrum, may appear in the local one. In the intermediate regime of a narrow but finite probe, it is possible that a cancellation of the contributions from Ψ^{λ} takes place between different points in space leading to a non-trivial localization of the absorption. The result will then be quite sensitive to the extent of the light beam.

3. The physical origin of exciton confinement

Both free-carrier and excitonic confinement effects are described by the SBE approach (6). In particular, the correlated energy spectrum in the low-density limit is given by eigenvalues of the polarization equation; the necessary ingredients are single-particle envelope functions $\psi_{i/j}$ and energy levels $\epsilon_{i/j}$, as well as the Coulomb matrix elements V in equations (7) and (8). These, in turn, are obtained from a numerical solution of the Schrödinger equation (in actual calculations we use a plane-wave representation; see [3]) with given confinement potential profile $V_c^{e/h}$ and bulk effective masses $m^{e/h}$ for electrons/holes. The explicit form of the Coulomb matrix elements entering our SBE is given by

$$V_{l_1 l_2 l_3 l_4} = \int \mathrm{d}\boldsymbol{r} \int \mathrm{d}\boldsymbol{r}' \; \psi^*_{l_1}(\boldsymbol{r})\psi^*_{l_2}(\boldsymbol{r}')V(\boldsymbol{r}-\boldsymbol{r}')\psi_{l_3}(\boldsymbol{r}')\psi_{l_4}(\boldsymbol{r}) \tag{34}$$

where $V(\boldsymbol{r}, \boldsymbol{r}')$ is the two-body Coulomb potential.

3.1. Quantum confinement

When no spatial variation of the dielectric constant exists in the structure, the two-body potential $V(\boldsymbol{r}, \boldsymbol{r}')$ entering equation (34) reduces to the usual Coulomb potential

$$V(\boldsymbol{r}, \boldsymbol{r}') = \pm \frac{e^2}{4\pi\varepsilon_0|\boldsymbol{r}-\boldsymbol{r}'|} \tag{35}$$

where ε_0 is the homegeneous dielectric constant of the material. Furthermore, the confinement potential is simply dictated by the conduction/valence band discontinuities $V_c^{e/h}(\boldsymbol{r})$ (quantum confinement), whose geometrical shape may be derived, e.g., from TEM images, as in [8]. The effective potential induces a q1D free-carrier confinement, i.e., a localization of the electron and hole envelope functions $\psi_{i/j}$ which, in turn, results in an increase of the Coulomb matrix elements in (34), and hence the enhancement of E_b with respect to the bulk case (excitonic confinement).

3.2. Dielectric confinement

For a spatially modulated dielectric constant $\varepsilon(\boldsymbol{r})$, the Coulomb interaction between two charged particles—electrons and/or holes—sited at positions $\boldsymbol{r}$ and $\boldsymbol{r}'$ is given by

$$V^0(\boldsymbol{r}, \boldsymbol{r}') = \pm e^2 G(\boldsymbol{r}, \boldsymbol{r}') \tag{36}$$

where $G(\boldsymbol{r}, \boldsymbol{r}')$ is the Green's function of the effective Poisson equation:

$$\boldsymbol{\nabla}_r \cdot \varepsilon(\boldsymbol{r})\boldsymbol{\nabla}_r G(\boldsymbol{r}, \boldsymbol{r}') = -\delta(\boldsymbol{r}-\boldsymbol{r}'). \tag{37}$$

Therefore, the space dependence of $\varepsilon(\boldsymbol{r})$ modifies $G(\boldsymbol{r}, \boldsymbol{r}')$ with respect to the homogeneous case, equation (35); the Green's function $G(\boldsymbol{r}, \boldsymbol{r}')$—and thus the corresponding potential V^0—depends, in general, both on the relative coordinate $\boldsymbol{r}-\boldsymbol{r}'$ and on the centre-of-mass coordinate $(\boldsymbol{r}+\boldsymbol{r}')/2$. This, in turn, gives rise to a space-dependent self-energy term [22]:

$$\Delta\epsilon(\boldsymbol{r}) = \frac{e^2}{2} \lim_{\boldsymbol{r}' \to \boldsymbol{r}} \left[G(\boldsymbol{r}, \boldsymbol{r}') - G^B(\boldsymbol{r}, \boldsymbol{r}') \right] \tag{38}$$

where

$$G^B(\boldsymbol{r}, \boldsymbol{r}') = \frac{1}{4\pi\epsilon(\boldsymbol{r})|\boldsymbol{r}-\boldsymbol{r}'|} \tag{39}$$

is the (local) bulk solution of (37). The self-energy $\Delta\epsilon$ can be regarded as a local correction (equal for electrons and holes) which adds to the confining potential $V_c^{e/h}$ in determining

the single-particle envelope functions $\Psi_{i/j}$ and the corresponding energy levels $\epsilon_{i/j}$. From a physical point of view, such terms describe the Coulomb interaction between the carrier and the distribution of polarization charges induced—by the carrier itself—at the dielectric interfaces. This effect is often described in terms of classical image charges.

As illustrated in section 6, the effect of dielectric confinement on the single-particle properties is not negligible but it is usually dominated by quantum-confinement effects. In contrast, the presence of dielectric mismatch is found to play a crucial role in modifying the excitonic properties of the system. This is due to the strong increase of the Coulomb matrix elements in (34), which is mainly ascribed to the modifications due to dielectric mismatch of the Green's function G in equation (36).

Generally speaking, the main ingredient for a quantitative evaluation of dielectric confinement effects—both single-particle and excitonic—is the two-body Green's function introduced in (36). This can be obtained from a numerical solution of the Poisson equation (37), that we also perform in terms of a plane-wave expansion with periodic boundary conditions [23].

4. Coulomb-induced suppression of band-edge singularities

In this section we review Coulomb-correlation effects on the global optical spectra of realistic QWR structures [3, 21]. By means of the theoretical scheme presented in section 2 we have investigated realistic V- as well as T-shaped wire structures. In particular, here we show results for the GaAs/AlGaAs V-shaped wire structure of reference [8].

(a) *Excitonic absorption regime*. Let us start by considering the optical response of the system in the low-density limit. In figure 1 we show the linear absorption spectra obtained when taking into account the lowest wire transition only. Results of our Coulomb-correlated (CC) calculation are compared to those from the free-carrier (FC) model. As we can see, electron–hole correlation introduces two important effects. First, the excitonic peak arises below the onset of the continuum, with a binding energy of about 12 meV, in excellent agreement with experiments [8]. Second, and more important, one finds a strong suppression of the 1D DOS singularity. A detailed analysis of the physical origin of such suppression [3] has shown that the quantity which is mainly modified by CC is the oscillator strength (OS). In figure 2 the ratio between the CC and FC OS is plotted as a

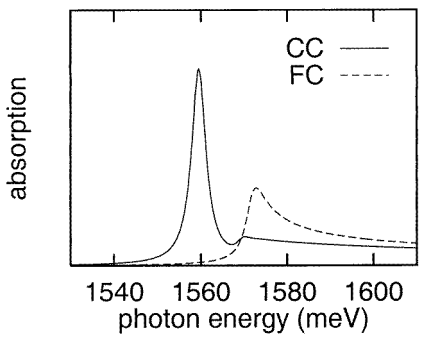

Figure 1. Linear absorption spectra of a realistic V-shaped wire structure. Solid curve: Coulomb-correlated (CC) result; dashed curve: free-carrier (FC) result. Here only the first electron and hole subbands are included for clarity (for the full 12-subband spectrum, see figure 3). After reference [21].

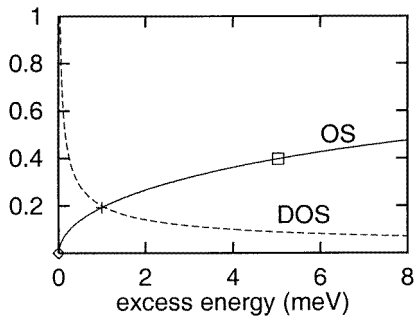

Figure 2. The oscillator strength (OS) ratio and density of states (DOS) versus excess energy; corresponding to the Coulomb-correlated absorption spectrum of figure 1 (solid curve). After reference [21].

function of excess energy (solid curve); this ratio is always less than one and goes to zero at the band edge. Such vanishing behaviour is found to dominate the 1D DOS singularity and, as a result, the absorption spectrum exhibits a regular behaviour at the band edge (solid curve in figure 1).

(b) *Gain regime*. Most of the potential QWR applications, i.e., 1D lasers and modulators, operate in strongly non-linear response regimes [1]. In such conditions, the above linear response analysis has to be generalized taking into account additional factors such as (i) screening effects, (ii) band renormalization, and (iii) phase-space filling.

Figure 3 reports quantitative results for non-linear absorption spectra of realistic V-shaped wire structures at different carrier densities at room temperature. As a reference we also show the results obtained by including the lowest subband only (figure 3(a)). In the low-density limit (case A: $n = 10^4$ cm^{-1}) we clearly recognize the excitonic peak. With increasing carrier density, the strength of the excitonic absorption decreases due to phase-space filling and screening of the attractive electron–hole interaction, and moreover the band renormalization leads to a red-shift of the continuum. At a density of 4×10^6 cm^{-1} (case D) the spectrum already exhibits a negative region corresponding to stimulated emission, i.e. a gain regime. As desired, the well pronounced gain spectrum extends over a limited energy region (smaller than the thermal energy); however, its shape differs considerably from the ideal FC one (the

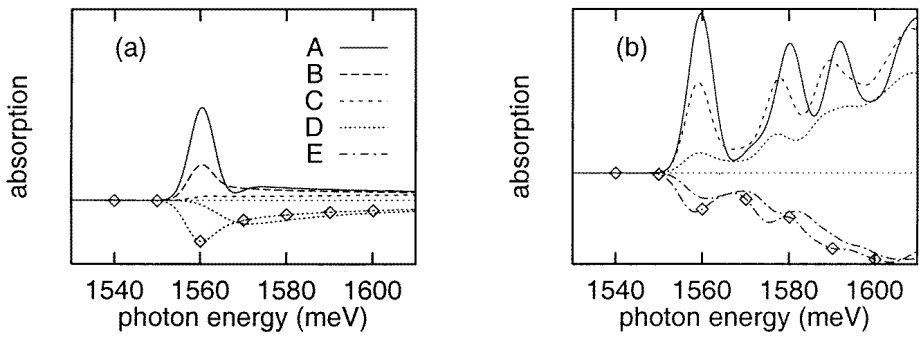

Figure 3. Non-linear absorption spectra of the V-shaped quantum wire of figure 3: (a) the single-subband case; (b) the realistic 12-subband case. After reference [21].

curve marked with diamonds in the same figure). In particular, the band-edge singularity in the ideal FC gain spectrum is clearly smeared out by electron–hole correlation. The overall effect is a broader and less pronounced gain region.

Finally, figure 3(b) shows the non-linear spectra corresponding to the realistic case of a 12-subband V-shaped wire. In comparison with the single-subband case (figure 3(a)), the multisubband nature is found to play an important role in modifying the typical shape of the gain spectra, which for both CC and FC models turns out to extend over a range much larger than that of the single-subband case for the present wire geometry. In addition, the Coulomb-induced suppression of the single-subband singularities, here also due to intersubband-coupling effects, tends to reduce the residual structures in the gain profile. Therefore, even in the ideal case of a QWR with negligible disorder and scattering-induced broadening, our analysis indicates that, for the typical structure considered, the shape of the absorption spectra over the whole density range differs considerably from the sharp FC spectrum of figure 1.

5. Shape-independent scaling of excitonic binding

As discussed in the previous section, the single-particle band-edge singularity of q1D systems is suppressed by virtue of electron–hole interaction, and the oscillator strength is transferred to the bound (below-band-gap) excitonic states which, for relatively low carrier densities, dominate the optical response of the system. To exploit such excitonic absorption in opto-electronic devices one needs to achieve a large exciton binding energy E_b compared to the thermal one; indeed, this has become a crucial goal in the field of semiconductor nanostructures. In this section, we discuss the intrinsic limitations of E_b for realistic QWRs.

For a given confinement length (i.e., given electron–hole Coulomb interaction energy), E_b results as a balance between the kinetic energy $\langle K \rangle$ and the Coulomb energy $\langle V \rangle$ (here and throughout this section, the symbol $\langle \cdots \rangle$ denotes the expectation value over the exciton ground state). The ratio $\alpha = \langle V \rangle / \langle K \rangle$ is fixed to -2 in strictly 2D and 3D Coulomb systems by virtue of the virial theorem, so $E_b = -\frac{1}{2}\langle V \rangle$; therefore, even for realistic q2D structures, where the virial theorem does not hold due to the presence of a confining potential, we expect α to deviate only slightly from -2. In strictly 1D systems, instead, α is ill-defined because both $\langle V \rangle$ and $\langle K \rangle$ diverge. Therefore, it might be hoped that in q1D systems a more convenient ratio (i.e., larger α) could be obtained for properly designed structures.

In this spirit, in this section we review the theoretical analysis presented in [15], where a detailed investigation of excitonic confinement has been performed for a wide class of state-of-the-art GaAs/AlGaAs QWRs, to clarify whether geometrical tailoring of the structure could be used to enhance the binding energy. We focused on realistic V- as well as T-shaped wire (V-wire and T-wire) structures; for both geometries, two different sets of conduction and valence band offsets (V_c^e and V_c^h, respectively) have been considered, in order to simulate both low-x $Al_xGa_{1-x}As$ and pure AlAs barrier compositions. In total, we consider four sets of samples, which we label V1, V2, T1, T2, where V (T) refers to the wire shape, and 1 (2) refers to the low (high) barriers. For V-wires, we start from the reference-sample TEM profile of reference [8], and magnify or reduce both confinement directions by the same scale factor. Each sample is characterized by the confinement length L_V at the bottom of the V-shaped region. For T-wires, we consider a set of samples with several values of the parent QW width, L_T, which includes the samples of reference [11]. The wire geometries are sketched as insets in figure 4, and the material parameters characterizing the four QWR sets are given in [15].

Figure 4 shows E_b and the corresponding mean potential energy $\langle V \rangle$ as functions of the characteristic size parameter of the wire, L_V or L_T. As expected, both binding and potential energies increase with decreasing L_V or L_T; for samples V2 and T2, corresponding to AlAs

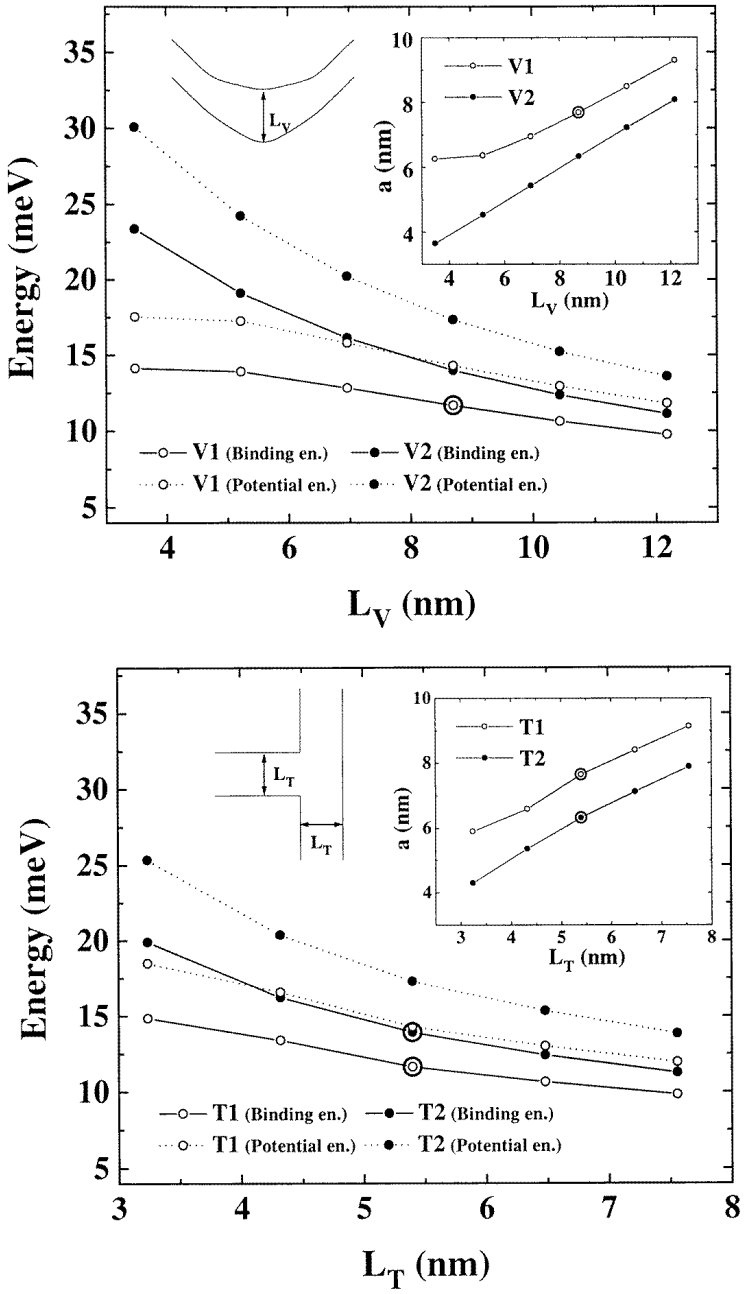

Figure 4. The exciton binding energy E_b and mean potential energy $\langle V \rangle$ of different V-wires (top) and T-wires (bottom). Full dots indicate high-barrier samples and empty dots indicate low-barrier samples, according to the keys. The wire geometries are sketched in the left-hand insets, with indications of the relevant geometrical parameters. The calculated effective exciton Bohr radius, a, versus the relevant geometrical parameter is shown in the right-hand inset in each case. The circled points refer to sample parameters corresponding to reference [8] (V-wires) and reference [11] (T-wires). After reference [15].

barriers, the excitonic binding energy is larger compared to the case of low-barrier samples V1 and T1.

Two important features result from figure 4. First, a given value of E_b corresponds to rather different values of L_V and L_T (note the different scale). Therefore, such size parameters are not adequate to characterize the actual exciton confinement. To introduce a more appropriate quantity, we define an effective exciton Bohr radius

$$a = \left\langle \frac{1}{r} \right\rangle^{-1} \tag{40}$$

whose inverse is clearly proportional to the potential energy and, for a 3D bulk semiconductor, coincides with the usual exciton Bohr radius a_0. The insets in figure 4 show a as a function of the relevant geometrical parameter, L_V or L_T. A same value of a corresponds to different values of L_V and L_T, with L_V always larger than L_T. Note that samples with similar binding energies correspond to similar values of a (see, e.g., the circled points, to be discussed below). The second feature resulting from figure 4 is that the ratio of binding to potential energy is rather constant (shape and barrier independent), and relatively close to one. This tells us that for all samples considered the mean kinetic energy $\langle K \rangle$ is much smaller (about four times) than the potential energy.

Both features indicate a shape-independent scaling of the exciton binding energy. When we plot the binding energy E_b versus the corresponding exciton radius a for all samples (figure 5) we obtain a universal (shape- and barrier-independent) curve, $E_b \sim 1/a$. A universal scaling of the mean potential and kinetic energy is apparent in the $\langle V \rangle$–$\langle K \rangle$ plot reported in the inset of figure 5; to a very good approximation, all sets of points for V- and T-wires fall on a straight line with slope α very close to 4. For comparison, we have performed analogous calculations for a set of QWs, and the results are also shown in figure 5. We find that E_b scales with a similarly to the case for q1D structures, although with a different prefactor. If $\langle V \rangle$ is plotted versus $\langle K \rangle$ (see the inset), the slope is now 2 within numerical accuracy.

We can therefore conclude that, for q1D structures in the strong-confinement regime considered here, the potential-to-kinetic-energy ratio is enhanced with respect to the value imposed by the conventional virial theorem for 3D and ideal 2D systems, which we find to be also followed by QWs of comparable confinement lengths. In this respect, our findings confirm that q1D confinement is indeed advantageous for the purpose of obtaining enhanced exciton binding, and provide a general and quantitative prescription for tailoring E_b by tuning the effective exciton Bohr radius a through the geometrical size parameters.

At the same time, however, the universal scaling law shown in figure 5 sets a clear limit for the possible effects of choosing different shapes of the wire cross-section, as long as they correspond to similar values of the effective Bohr radius a. For a given value of a, there is no hope of further increasing E_b by tailoring the potential-to-kinetic-energy ratio α through the geometry of the confining profile.

6. Enhanced exciton binding caused by remote dielectric confinement

The previous analysis shows that the bulk exciton binding energy E_b can be strongly enhanced by confining electron and hole wavefunctions in nanostructures of low dimensionality (quantum confinement), the most promising systems being q1D structures; within GaAs-based samples, however, the observed values of E_b are still well below the room-temperature thermal energy, kT_{room}.

As mentioned in the introduction, in principle the electron–hole Coulomb attraction can be enhanced by growing layered structures with a strong dielectric mismatch [17]. Unfortunately,

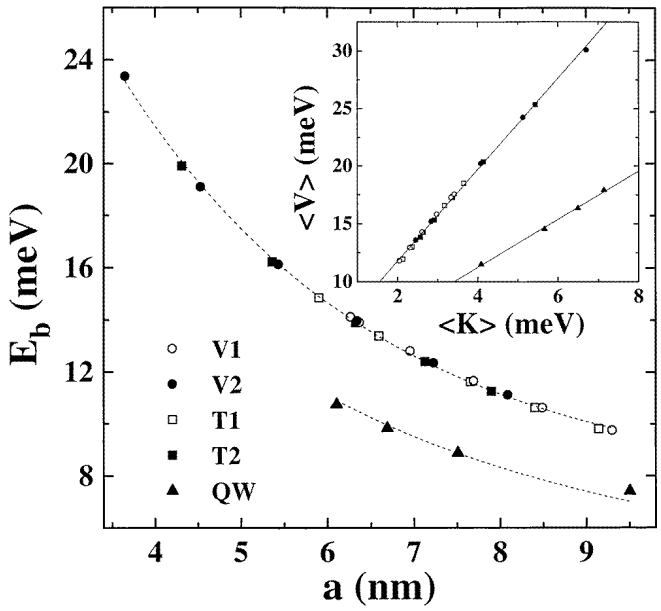

Figure 5. The exciton binding energy, E_b, versus the effective exciton Bohr radius, a, for the four sets of V- and T-wires, and for the set of QWs. Dashed curves are fittings to a $1/a$ form. The inset reports the average potential versus kinetic energy, falling on a straight line with slope $\alpha \simeq 4$ for all wire samples. Results for QW structures are also shown for comparison; in this case $\alpha \simeq 2$. Solid lines are linear fits to the calculated points. After reference [15].

in practice interfaces between III–V semiconductors and materials with very different dielectric constants, such as oxides, are usually very far from the excellent optical quality of the conventional ones. Recently, we have proposed an alternative approach [16] based on the observation that *quantum and dielectric confinement can be spatially separated*, since they are effective over different length scales. This can be accomplished for QWRs by adding *remote* insulating layers to the conventional structure (remote dielectric confinement, RDC); in the new structure, the electron and hole wavefunctions are confined by the inner, lattice-and-dielectric-matched GaAs/AlGaAs interfaces; the outer AlGaAs/oxide interfaces, owing to the strong dielectric mismatch, provide polarization charges, thereby enhancing the electron–hole interaction, as discussed in section 3.2.

In this section we review results obtained for GaAs/AlGaAs-based structures, and we show that RDC allows for a very large increase of E_b, up to three times the binding energy of the corresponding conventional structure, without degrading the good optical properties typical of these systems. As prototypical samples, we consider once more the two GaAs-based V-shaped and T-shaped wires of references [8] and [11]. Starting from these geometries, we design hybrid structures, adding oxide layers at some distance from the inner GaAs region. The oxide layers are characterized by a small dielectric constant, that we take equal to 2 [24].

We first consider a V-shaped structure, to which we add two oxide layers, below and above (see figure 6(a)), at a distance L from the GaAs/AlAs interfaces. For the sample shown in figure 6(a), we find $E_b = 29.3$ meV, to be compared with 13 meV for the conventional (i.e., with no oxide layers) structure. Figure 6(a) shows that the origin of this dramatic enhancement is the large polarization of the AlAs/oxide interfaces induced by the hole charge density; the polarization is larger in the region where the hole is localized, and is more pronounced at the

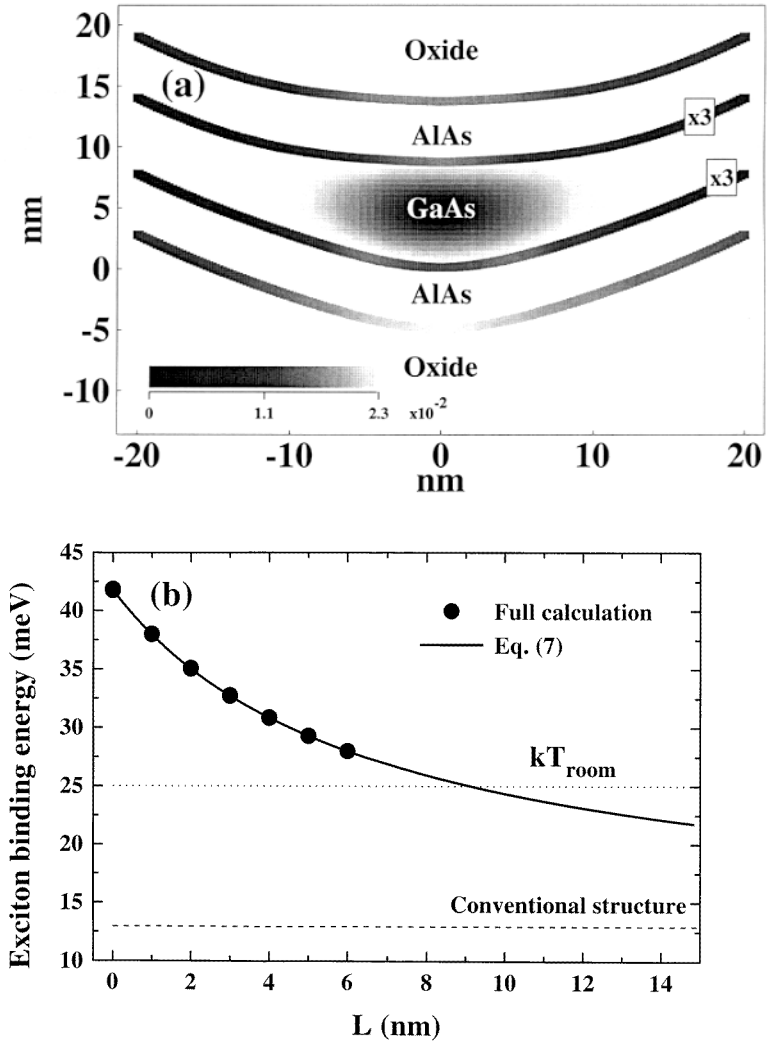

Figure 6. (a) A cross-section of a hybrid V-wire showing the interface polarization charge induced by the charge-density distribution of the lowest-subband hole; the oxide layers are at $L = 5$ nm from the GaAs/AlAs interfaces. (b) E_b versus the distance of the oxide layers from the internal interfaces, L. Solid dots: full calculation. Solid curve: equation (41) with $L_0 = 6.56$ nm. Dashed line: the energy E_0 of the corresponding conventional structure (no oxide layers). Dotted line: the thermal energy at $T_{\text{room}} = 300$ K. After reference [16].

lower interface, due to the larger curvature. A small polarization charge is also induced at the GaAs/AlAs interface, due to the small dielectric mismatch. Note that quantum confinement localizes the wavefunction well within the inner interfaces; therefore, the possible disorder of the AlAs/oxide interface does not affect the electron and hole wavefunctions.

In figure 6(b) we show the calculated E_b for selected values of L. We also show, for comparison, the calculated binding energy for the conventional structure, E_0, and the room-temperature thermal energy. E_b is maximum when the oxide layer is at minimum distance: it is enhanced by a factor larger than 3 with respect to E_0, and it is well above kT_{room}. It is

important to note that E_b decreases slowly with L, and is still significantly larger than kT_{room} at $L = 6$ nm. Since E_b is the result of the Coulomb interaction of, say, the electron with the hole *and* the polarization charge which is excited at a distance $\sim L$ by it, we intuitively expect E_b to decay as L^{-1}, with a typical decay length L_0 comparable to the Bohr radius in the wire [15]; this, in turn, is of the order of the confinement length. Indeed, figure 6(b) shows that E_b is very well interpolated by

$$E_b(L) = E_0 + \frac{E_b(0)}{1 + L/L_0} \tag{41}$$

with $L_0 = 6.56$ nm. Note that E_b crosses kT_{room} when L is as large as 9 nm.

Let us now discuss results for a GaAs/AlAs structure formed by GaAs parent QWs of the same width, and AlAs barriers (see figure 7(a)). An oxide layer is added on top of the exposed surface at a distance L from the underlying QW. Note that, in this case, an oxide layer is present only on one side of the structure. As in the previous case, a strong polarization charge forms at the AlAs/oxide interface, with a maximum in the region of the hole wavefunction confinement. A small polarization charge is also present at the GaAs/AlAs interface, peaked around the corners of the intersecting QWs. In figure 7(b) we show the calculated E_b versus L. The binding energy for the conventional structure, E_0, and the room-temperature thermal energy are also shown for comparison. As in the V-wire case, E_b is maximum at $L = 0$, where it is enhanced by a factor of 1.5 with respect to E_0, and decreases slowly with L. Although E_b is smaller than in the previous case, for the smallest L-values E_b is still of the order of kT_{room}. It is important to note that the reduced effect of dielectric confinement with respect to that of the previous example is just due to the presence of a single oxide layer, i.e., geometric effects due to different wire cross-sections play a minor role. In fact, despite the very different geometry, E_b decays with L in the same way in both cases. As shown in figure 7(b), in this case also E_b is very well interpolated by equation (41) with $L_0 = 7.55$ meV, which is still of the order of the carrier confinement length.

We finally comment on the effect of the self-energy term $\Delta\epsilon$ introduced in section 3.2 (see equation (38)). We have compared the full calculations discussed above with calculations performed neglecting $\Delta\epsilon(\boldsymbol{r})$ in the single-particle potential. For the V-shaped structure we have verified that the self-energy contribution tends to increase E_b, but it is so small (<0.2 meV) that the two results cannot be distinguished on the scale of figure 6(b). In the T-wire case, on the other hand, the effect of the self-energy term is qualitatively and quantitatively different, as can be seen from figure 7(b); in fact, the self-energy contribution amounts to ~ 1 meV at the smallest L, and tends to reduce E_b. This is a consequence of the interplay between the dielectric confinement and the shallow quantum confinement of these structures.

In summary, the above results show that a dramatic enhancement of the exciton binding in GaAs-based quantum structures is expected to be induced by remote insulating layers, bringing E_b into the range of the room-temperature thermal energy. Although, in real structures, several nanometre-wide spacer layers might be necessary to maintain the excellent optical efficiency typically obtained within the GaAs-based technology, we have shown that E_b scales slowly with the width of the spacer layer, thus allowing the design of nanostructures that should be compatible with optical efficiency but with a very large exciton binding energy.

7. Local spectroscopy of coupled QWR structures

All of the results presented so far are obtained in the so-called global excitation regime discussed in section 2.1, i.e., they are induced by homogeneous light fields treated within the dipole approximation. In this section we review recent calculations of local absorption spectra for

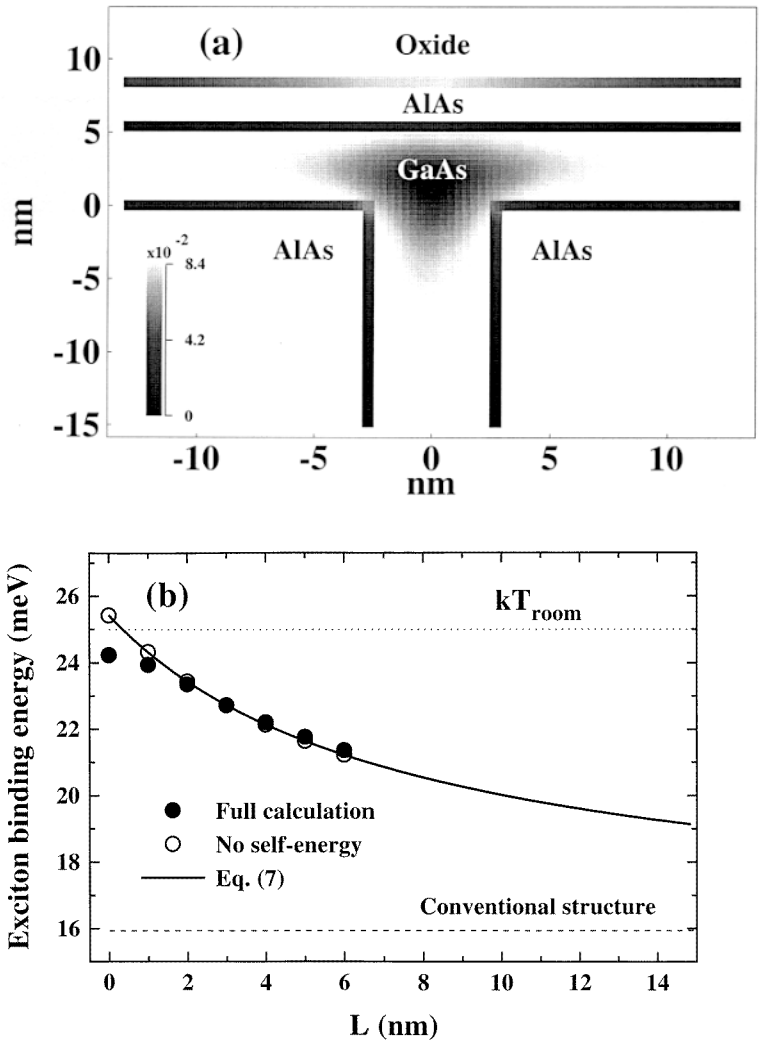

Figure 7. (a) As figure 6(a), but for a hybrid T-wire. The QW widths are 5.4 nm and $L =$ nm. (b) E_b versus L including (solid dots) and neglecting (empty dots) the self-energy contribution. Solid curve: equation (41) with $L_0 = 7.55$ nm. Dashed line: energy E_0 of the corresponding conventional structure (no oxide layers). Dotted line: thermal energy at $T_{\text{room}} = 300$ K. After reference [16].

coupled QWRs structures, based on the space-dependent formulation presented in section 2.2.

The appearance of optical spectroscopies with high spatial resolution, combined with improved control in the fabrication of semiconductor nanostructures, has made it possible to study the optical response of individual quantum wires and dots. When the resolution is reduced to below the diffraction limit [25], it is possible not only to investigate individual nanostructures, but also to study Coulomb-correlation phenomena and new effects of coherence and coupling between spatially separated quantum states. In conventional optical experiments, the light field is essentially constant in amplitude and phase over the spatial extent of the relevant quantum mechanical states. In contrast, microprobe techniques make use of highly

inhomogeneous light fields: in analogy with ultrafast time-resolved spectroscopies [5], that have shown the importance of phase coherence in the quantum mechanical time evolution of photoexcited carriers, it may be expected that spatial interference of quantum states plays a dominant role when variations of the EM field occur on an ultrashort length scale.

On the theoretical side, however, few studies have so far investigated the response under these conditions; most studies focus on the near-field distribution of the EM field [26] and its interaction with arrays of point-like particles [27]; only recently has the response to an inhomogeneous EM field in a semiconductor quantum dot been studied within the single-particle approximation [28].

Since the phase of the relevant quantum states is dominated by electron–hole correlations on the scale of the exciton Bohr radius, to emphasize potential Coulomb-coupling effects we show results obtained for a Gaussian light beam with $\sigma = 10$ nm (close to the Bohr radius in GaAs), although near-field scanning optical microscopy (NSOM) experiments on semiconductors are currently still limited to higher values of σ. As a prototype system showing non-local effects we consider two coupled semiconductor T-shaped wires [29] (see the inset in figure 8(a)). In order to obtain spatially separated transitions we consider an asymmetric structure; the distance between the wires is chosen to allow Coulomb coupling between them. The single-particle electron and hole ground states (E1, H1) are localized in the widest wire (right-hand wire, RW) and the second bound states (E2, H2) in the left-hand wire (LW).

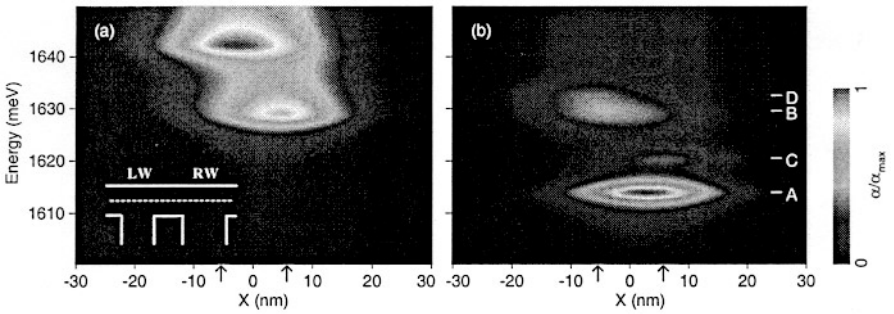

Figure 8. Local absorption $\alpha(\boldsymbol{R}, \hbar\omega)$ as a function of photon energy and beam position for a coupled T-wire nanostructure. The spectra are calculated (a) within the single-particle approximation, and (b) including the electron–hole Coulomb correlation. Here, $\sigma = 10$ nm. The X-coordinate represents the beam position along the dashed line in the inset; the centres of the wires are indicated by arrows. The vertical GaAs stems are 5.4 nm and 6.0 nm wide, separated by a 5.4 nm AlAs layer; the horizontal well is 5.4 nm wide. The labels A, B, C, D identify the main structures (see the text).

Figure 8 shows the local absorption $\alpha(\boldsymbol{R}, \hbar\omega)$ (see equation (30) in section 2.2) as a function of photon energy and with the beam position sweeping across the structure (see the inset). If the electron–hole interaction is neglected (figure 8(a)) the spectrum is essentially composed of two structures, both with the inverse-square-root high-energy tail typical of the 1D free-particle density of states; the signal from the E1–H1 transition is spatially located on the RW while a second peak, located on the LW, stems from the E2–H2 transition; in this uncorrelated case the influence of spatially indirect transitions (E1–H2, E2–H1) is negligible.

The correlated carrier spectrum (figure 8(b)) is red-shifted by the excitonic binding energy [15] ($\sim$14 meV), and the corresponding continuum is strongly suppressed by electron–hole correlation [3]. The two main peaks (A and B) still have their largest contributions in the RW and LW, respectively; however, two weaker structures, C and D, appear which are strongly localized in either wire and have no equivalent in the uncorrelated spectrum. Peak A

is the ground-state exciton (E1–H1), and is mainly localized in the RW, but has a significant intensity also in the LW. Peak C also originates from the RW where a second bound exciton is introduced in the presence of Coulomb coupling with the LW. Peak B stems from several exciton states, with a major component in the E2–H2 transition on the LW. The shoulder D (mostly a E2–H1 transition) is very intense in the local spectrum centred on the LW, completely absent when the beam is centred on the RW, and very reduced in the global spectrum.

We stress that the strong localization of D comes from the interference between positive and negative regions of the exciton wavefunction Ψ^{λ} (see equation (30)), whose cancellation depends on the position of the beam.

In summary, we have shown that when the spatial resolution of the optical excitation pulse becomes comparable to the exciton Bohr radius, the local optical absorption is dominated by electron–hole correlations. Similar calculations performed on terraces originating from QW thickness fluctuations confirm that these phenomena are general, and especially significant for coupled nanostructures when they are investigated with spatial resolution of the order of the Bohr radius. The breaking of far-field selection rules that is expected to occur at such resolutions might then give insight into Coulomb-correlation and coherence phenomena.

Acknowledgments

We are grateful to R Cingolani, L Sorba and E Kapon for stimulating discussions. This work was supported in part by the MURST-40% program 'Physics of Nanostructures' and by the EC Commission through the TMR Network 'Ultrafast Quantum Optoelectronics'.

References

[1] For recent reviews see
Sakaki H, Someya T, Akiyama H, Nakamura Y, Kondo N and Kishimoto D 1997 *Proc. 5th Int. Mtg on Optics of Excitons in Confined Systems; Phys. Status Solidi* a **164** 241
Goldoni G, Rossi F and Molinari E 1997 *Proc. 5th Int. Mtg on Optics of Excitons in Confined Systems; Phys. Status Solidi* a **164** 265
[2] Ogawa T and Takagahara T 1991 *Phys. Rev.* B **43** 14 325
Ogawa T and Takagahara T 1991 *Phys. Rev.* B **44** 8138
[3] Rossi F and Molinari E 1996 *Phys. Rev. Lett.* **76** 3642
Rossi F and Molinari E 1996 *Phys. Rev.* B **53** 16 462
[4] Haug H and Koch S W 1994 *Quantum Theory of the Optical and Electronic Properties of Semiconductors* 3rd edn (Singapore: World Scientific)
[5] Shah J 1996 *Ultrafast Spectroscopy of Semiconductors and Semiconductor Nanostructures* (Berlin: Springer)
[6] Schöll E (ed) 1998 *Theory of Transport Properties of Semiconductor Nanostructures* (London: Chapman & Hall)
[7] Kapon E, Hwang D M and Bhat R 1989 *Phys. Rev. Lett.* **63** 430
[8] Rinaldi R *et al* 1994 *Phys. Rev. Lett.* **73** 2899
[9] Grundmann M, Christen J, Bimberg D and Kapon E 1995 *J. Nonlin. Opt. Phys. Mater.* **4** 99 and references therein
[10] Pfeiffer L, West K W, Stormer H L, Eisenstein J P, Baldwin K W, Gershoni D and Spector J 1990 *Appl. Phys. Lett.* **56** 1697
Wegscheider W, Pfeiffer L, West K and Leibenguth R E 1994 *Appl. Phys. Lett.* **65** 2510
[11] Someya T, Akiyama H and Sakaki H 1996 *Phys. Rev. Lett.* **76** 2965
[12] Gislason H, Langbein W and Hvam J M 1996 *Appl. Phys. Lett.* **69** 3248
[13] Loudon R 1959 *Am. J. Phys.* **27** 649
Elliot R J and Loudon R 1959 *J. Phys. Chem. Solids* **8** 382
Elliot R J and Loudon R 1960 *J. Phys. Chem. Solids* **15** 196

[14] See, e.g.,
Bastard G 1988 *Wave Mechanics Applied to Semiconductor Heterostructures* (Les Ulis: Les Editions de Physique) ch IV and references therein
[15] Rossi F, Goldoni G and Molinari E 1997 *Phys. Rev. Lett.* **78** 3527
[16] Goldoni G, Rossi F and Molinari E 1998 *Phys. Rev. Lett.* **80** 4995
[17] Keldysh L V 1979 *Pis. Zh. Eksp. Teor. Fiz.* **29** 716 (Engl. Transl. 1979 *JETP Lett.* **29** 658)
[18] Andreani L C and Pasquarello A 1990 *Phys. Rev.* B **42** 8928
[19] Mauritz O, Goldoni G, Rossi F and Molinari E 1999 *Phys. Rev. Lett.* **82** 847
[20] Kuhn T 1998 *Theory of Transport Properties of Semiconductor Nanostructures* ed E Schöll (London: Chapman & Hall) p 173
[21] Rossi F 1998 *Semicond. Sci. Technol.* **13** 147
[22] Inkson J C 1984 *Many Body Theory of Solids—An Introduction* (New York: Plenum) ch 9
[23] This approach can be relevant also for applications to other systems, including nanocrystals embedded in glass matrices, where dielectric confinement effects are expected to be strong; see, e.g.,
Alivisatos A P 1996 *Science* **271** 933
[24] This is just intended as a typical value: oxides that could be of practical relevance—see, e.g.,
Fiore A, Berger V, Rosencher E, Bravetti P and Nagle J 1998 *Nature* **391** 463
have similar or smaller values. The value of the dielectric constant could be made even smaller if one could take advantage of interfaces with air.
Tikhodeev S G, Gippius N A, Yablonskii A L, Dzyubenko A B, Kulik L V, Kulatovskii V D and Forchel A 1997 *Phys. Status Solidi* a **164** 179
[25] See, e.g.,
Hess H F, Betzig E, Harris T D, Pfeiffer L N and West K W 1994 *Science* **264** 1740
[26] Chang R, Wei Pei-Kun, Fann W S, Hayashi M and Lin S H 1997 *J. Appl. Phys.* **81** 3369
[27] Hanewinkel B, Knorr A, Thomas P and Koch S W 1997 *Phys. Rev.* B **55** 13 715
[28] Bryant G W 1998 *Appl. Phys. Lett.* **72** 768
[29] Recent NSOM studies of T-shaped wires, focusing on characterization of the structures, include
Grober R D, Harris T D, Trautman J K, Betzig E, Wegscheider W, Pfeiffer L and West K 1994 *Appl. Phys. Lett.* **64** 1421
Harris T D, Gershoni D, Grober R D, Pfeiffer L, West K and Chand N 1996 *Appl. Phys. Lett.* **68** 988